RIGA TECHNICAL UNIVERSITY

Matīss Maltisovs

OPERATING METHODS OF HIGH VOLTAGE BISTABLE SMART GLASS ELECTRONICS SYSTEMS

Summary of the Doctoral Thesis

RTU Press
Riga 2022

RIGA TECHNICAL UNIVERSITY
Faculty of Electronics and Telecommunications
Institute of Radioelectronics

Matīss Maltisovs
Doctoral Student of the Study Programme "Electronics"

OPERATING METHODS OF HIGH VOLTAGE BISTABLE SMART GLASS ELECTRONICS SYSTEMS

Summary of the Doctoral Thesis

Scientific supervisor
Assoc. Professor *Dr. sc. ing.*
DMITRIJS PIKUĻINS

RTU Press
Riga 2022

Maltisovs M. Operating Methods of High Voltage Bistable Smart Glass Electronics Systems. Summary of the Doctoral Thesis. – Riga: RTU Press, 2022. – 47 pages.

Printed accordingly with the decision of the Promotion Council P-08 of December 07 2021, Minutes No. 5.

https://doi.org/10.7250/9789934227448
ISBN 978-9934-22-744-8

DOCTORAL THESIS PROPOSED TO RIGA TECHNICAL UNIVERSITY FOR THE PROMOTION TO THE SCIENTIFIC DEGREE OF DOCTOR OF ENGINEERING SCIENCES

To be granted the scientific degree of Doctor of Engineering Sciences (*Ph. D*), the present Doctoral Thesis has been submitted for the defence at the open meeting of RTU Promotion Council on March 11, 2022 at the Faculty of Electronics and Telecommunications of Riga Technical University, Āzenes street 12, room 201.

OFFICIAL REVIEWERS

Asoc. Professor *Dr. sc. ing.* Andis Supe
Riga Technical University

Professor *Dr. phys.* Mārtiņš Rutkis
University of Latvia, Institute of Solid State Physics

Professor *Ph. D.* Timothy D. Wilkinson
University of Cambridge, Great Britain

DECLARATION OF ACADEMIC INTEGRITY

I hereby declare that the Doctoral Thesis submitted for the review to Riga Technical University for the promotion to the scientific degree of Doctor of Engineering Sciences is my own. I confirm that this Doctoral Thesis had not been submitted to any other university for the promotion to a scientific degree.

Matiss Maltisovs ..... (signature)
Date: .....

Summary of the Doctoral Thesis has been written in English. It consists of an Introduction; 2 chapters; Conclusions; 32 figures; 9 tables; the total number of pages is 47. The Bibliography contains 24 titles.

DEDICATION

To my wife Rūta

and my both sons Krišjānis and Mārtiņš

ACKNOWLEDGEMENTS

First of all, I would like to thank my supervisor Assoc. Professor. *Dr. sc. ing.* Dmitrijs Pikuļins for the management, valuable advice and support that provided motivation and new ideas in the development of the work.

I would like to thank former colleagues from *EuroLCDs* for support, discussions, assistance in the preparation of samples and in performing the measurements: Ainārs Ozols, Ilmārs Sekacis, Kristaps Moruss, Jānis Kļaviņš, Jānis Kondratjevs, Kārlis Krūmiņš, Kristiāns Krūmiņš, Rolands Šķirmants, Dainis Backāns, Jānis Zālītis, Artūrs Jankevičs, Mikus Matisons, Jānis Čerņavskis, Mārtiņš Rudzājs, Lāsma Vaita, Mārcis Ruzaiķis and Elīna Emare.

Big gratitude goes to the management of *HansaMatrix Innovation* for giving the opportunity on development of the doctoral thesis and research papers: Ilmārs Osmanis, Krišs Osmanis and Aija Kopštāle. I would also like to thank my colleagues and former colleagues for support in hardware design, manufacturing and testing: Valters Skrastiņš, Linards Grigāns, Uģis Sirmelis, Roberts Gotlaufs, Pāvels Ivanovs and Mārcis Greitāns.

I would like to thank my parents — Juris and Solvita for believing in my dreams and being supportive when it was the most needed.

Last, but most importantly, my heartfelt gratitude goes to my wife Rūta, who has accompanied me through my doctoral studies. I would like to thank my wife for her enduring love and support during the highs and lows of the past several years.

ANNOTATION

Liquid crystal displays ($LCDs$) have been used by mankind on a daily basis for decades, but the demand for their integration and development of new products is only growing. One of the research directions is smart glass/windows, and, although they are known for more than 25 years, there are areas that still need to be researched. This Thesis focuses on *Smectic-A* (SmA) liquid crystals' (LCs) functional behaviour in order to understand if this will be the next generation product, that could improve society's daily life.

An in-depth literature review discusses existing studies, obtained experimental data and attempts to develop functional products. The main unresolved problems are highlighted, described in detail and solutions are offered.

The SmA LC is able to maintain two stable optical states: transparent and light scattering, without additional energy resources, allowing to save electricity costs. The optical properties of this liquid crystal are by far the best compared to the products available in the market, i. e. the light transmittance in transparent state is 85+ % and in scatter state < 2 %. Enabling the LC to be used for a variety of purposes, such as smart windows to scatter light on a sunny day or provide a sense of privacy in an open type office space.

In order to understand the potential of SmA LC in the smart glass/window technology, analysis of existing products was performed, a summary of an active smart glass/windows provided and a comparative study between them was made. In addition, an in-depth study of long-term functional stability was performed, during which the most popular types of defects were listed and analysed. Solutions for defect elimination and recommendations for optimization of switching systems and production processes are provided. A methodology for determining the electrical parameters of an LC has been developed in order to create an electrical simulation model and facilitate the development of electronic switching systems.

The results of the work are summarized and recommendations for the functional use of SmA LCs of various designs and sizes are provided.

CONTENTS

LIST OF SYMBOLS AND ABBREVIATIONS

LCD	Liquid crystal display
SmA	*Smectic-A* liquid crystal
LC	Liquid crystal
TV	Television
EC	Electrochromic device
PDLC	Polymer dispersed liquid crystal device
SPD	Suspended particle device
UV	Ultraviolet light
ITO	Indium tin oxide
$\mathbf{SiO_2}$	Silicon dioxide
Ns	Nematic liquid crystals
Ss	Smectic liquid crystals
n(r)	Unit vector, r — space coordinate, determines preferred molecule orientation
Sc	*Smectic-C* liquid crystal
ChLC	Cholesteric liquid crystal
Chiral	Unique ability to selectively reflect one component of circularly polarized light
$\boldsymbol{\varepsilon}$	LC cell dielectric material coefficient
IR	Infrared light
$\boldsymbol{\eta_o}$	Ordinary refractive index
$\boldsymbol{\eta_p}$	Polymer refractive index
RMS	Root mean square of measured voltage or consumed power
PVD	Physical vapour deposition
$\mathbf{LiCoO_2}$	Lithium cobalt oxide
$\mathbf{WO_3}$	Polycrystalline tungsten oxide
$\mathbf{\Omega/sq}$	ITO resistance value
PC	Personal computer
OPMP	Optical parameter measurement platform
AHV	Alternating high voltage source
E24 standard	System of preferred numbers (also called preferred values) derived for use in electronic components
Wh	Watt-hours
PDT	Product development testing
HALT	Highly accelerated life testing
QT	Qualification tests
FOAT	Failure oriented accelerated testing

$\boldsymbol{BIT}$	Burn in test
$\boldsymbol{PVC}$	Polyvinyl chloride, synthetic plastic polymer used for window frame manufacturing
$\boldsymbol{RC}$	Resistor—capacitor circuit
$\boldsymbol{C_{LC}}$	Liquid crystal capacitance
$\boldsymbol{R_S}$	LC cell series resistance (ITO resistance)
$\boldsymbol{R_P}$	LC cell parallel resistance (LC resistance)
$\boldsymbol{Q_C}$	Capacitor charge (LC cell charge)
$\mathbf{V_S}$	Supplied voltage
$\boldsymbol{E}$	Electric field intensity
$\mathbf{E_{br}}$	LC electrical breakdown value
$\boldsymbol{ICT}$	Information and communication technology
VATP	Ventspils high technology park
$\boldsymbol{SGD}$	Smart glass driver
2D	Two dimensional

1. GENERAL DESCRIPTION OF THE THESIS

1.1. Introduction

Nowadays Liquid crystal display (LCD) is an integral part of humans' everyday life. High demand for new and innovative LCD products force industry to develop and implement new types of *LCDs*. They are used in everything starting from smartphones and Television (TV) sets to washing machines. Liquid crystals (LCs) have far wider applications, one of them — smart or switchable glass, having voltage dependent optical properties which can be altered by application of specific electrical signals.

Smart glass technology has been studied for the last few decades; however, its demand is gathering innovation in raw materials, technologies and the possibilities for new applications across various sectors, e. g. smart windows.

Windows serve an important function in homes and commercial buildings. They let the light in and brightens the room, saving electricity costs. They provide heat and air conditioning, and other appliances must be used in order to adjust the comfort level. But windows are not the best insulating material for the cold season, and they are not something people typically associate with being a cutting-edge technology.

There are two primary types of smart glass, defined by whether or not their changeability requires an electrical signal:

- **Active devices (depends on the signal):**
  - Electrochromic (EC)
  - Polymer Dispersed Liquid Crystal ($PDLC$)
  - Suspended Particle Devices (SPD)
  - Other (e. g. bistable *Smectic-A* (SmA) LC devices)
- **Passive devices (does not depend on signal):**
  - Thermochromic
  - Photochromic

The main advantages of the smart glass are:

- **privacy** – a fast state change from clear to light scattering state and vice versa, low transmittance in opaque state, ability to replace curtains, shutter blinds, drapes;
- **cost savings** – no need for an additional cleaning equipment, saves costs for heating, air-conditioning and lighting, no costs of installing and maintaining motorized light screens, blinds or curtains;
- **ultraviolet (UV) protection** – blocks > 98 % of UV rays;
- **display and advertising** – can be used as a projection screen when switched to the light scattering state.

Over the past 50 years, many different studies have been conducted on and around *SmA LC* and their devices. Despite rapid technological development, *SmA LCDs* have not reached the market compared to other similar products such as *PDLC*. This begs the question: why?

- Existing studies do not provide detailed information about the conducted sample size, however in most cases it was $< 50 \times 50$ mm. This means that regardless of the technological possibilities, no technical solution has been found to successfully produce *SmA LC* devices of different sizes, i. e., such as 8×8 mm up to 300×400 mm or bigger.
- The driving methodology is discussed quite extensively, i. e., matrix-addressing with thermal and electric field effects [1], [2], electrode configurations [3], operating, switching characteristics [4], [5], electrohydrodynamic [6], etc. None of the studies fully addresses switching threshold frequencies for both states (light scattering and transparent) and from state to state. Also the frequency dependence of the switching speed and or light transmission is unknown.
- In addition to *LC* switching, specific issues are addressed, such as the use of different frequencies and signal amplitudes to obtain different levels of grey tones in a light scattering state. But the topics of switching sequence, pauses between state-state, pixel-pixel switching, their effect on light transmittance, etc. are not covered.
- No information is available about long term switching problems, defects. As well as no studies about *LC* defect analysis have been published, not to mention to finding solutions to resolve defects or prevent their appearance.
- Lack of theoretical studies and experiments to obtain an equivalent load model, i. e., to be able to replicate the *LCD* in electronic simulation environments with equivalent load, which would help to speed up the electronic design process of desired product more efficiently without iterative approaches and testing with real samples with high production costs.
- It is not known how the power consumption changes in relation to the area to be driven or the amount of the current required to switch an area of a certain *LCD* or pixel size. What is the power consumption for different *LC* cell types, designs?
- There is no information about differences in the thickness of the protective coatings, such as SiO_2, effect the switching speed, light transmittance, power consumption. Also, what is the effect on changes in indium tin oxide (ITO) resistance etc.?

1.2. Objectives of the Thesis

The purpose of this Thesis is to explore operational and electrical properties of the *SmA LC* cells, as well as gain an in-depth understanding of functional long-term stability. To achieve the goal, the following objectives have to be fulfilled:

- Explore the light transmittance and switching speed of *SmA LC* cells, depending on the switching frequency (Chapter 2.2, Section 2.2.1);
- Explore power consumption based on switching area (Chapter 2.2, Section 2.2.2);
- Explore switching differences between different *LC* cell design types (Chapter 2.3, Section 2.3.2);
- Explore equivalent load representation options for electronic sub-system simulations (Chapter 2.5, Sections 2.5.1-2.5.3);
- Explore *LC* defect types, their appearance reasons and possible solutions (Chapter 2.3 and 2.4.1).

Other active smart glass devices should be explored by reviewing and analysing other research topics on electrical and optical functionality, so they could be compared with *SmA LC* devices.

1.3. Scientific novelty and main results

The following list outlines the major contributions that have been made during writing this Doctoral Thesis:

- New capillary filling process was developed that successfully allows to fill different size (from 10 × 10 mm up to 300 × 400 mm) *SmA LC* cells.
- Optical parameter measurement platform (*OPMP*) and switching matrix devices was developed that are able to measure light transmittance, switching speed, viewing angle and switch up to 5 different design, type *SmA LC* cells to increase testing volume for future needs.
- For the first time *SmA LC* cell frequency response and its dependence on switching speed, light transmittance and power consumption has been studied.
- For the first time *SmA LC* cell equivalent load theoretical model approach has been studied.
- For the first time *SmA LC* cell long-term switching defect analysis has been performed.
- For the first time *SmA LC* cell defect resolving methodology has been proposed and tested (approbated).
- Industrial type *SmA LC* driver was designed with capability to simultaneously switch two *LC* cells in size up to 300 × 400 mm.

1.4. Theses to be defended

- It is possible to obtain in 300 × 400 mm *SmA LC* cell the parameters required for smart glass applications — light transmittance > 85 % and switching speed < 150 ms in transparent state, light transmittance < 2 % and switching speed < 1700 ms in scatter state by applying 100—240 V > 0.9 A DC balanced square wave control signal within 20—40 Hz range for transparent state and within 400—700 Hz range for scatter state.
- During long-term functional testing, switching > 1000 times between both optical states, the following visual defects appear in *SmA LC* cell, preventing further use in smart glass applications: non uniform active area, pronounced laser ablation lines, random *LC* clusters, wavy pixels' outline and rugged pixels' edges.
- Long-term functionality and visual stability of *SmA LC* cells could be improved by: switching parameter and sequence optimization — additional 1—5 s pauses in-between state-state, pixel-pixel switching; changing control signal to DC balanced sine wave, as well as temperature treatment, but trade-off must be found between visual performance, functional switching and complexity of electronics design.
- The performance of the *SmA* liquid crystals can be modelled with the experimentally obtained equivalent load theoretical model: $RS = 71\ \Omega$, $RP = 13\ \text{k}\Omega$, $C = 53$ nF, to understand electric functionality of 300 × 400 mm *SmA LC* cells within 100—240 V range, which can be adjusted to other sizes.

1.5. Approbation

The following papers have been published in scientific journals & conference proceedings:

- M. Maltisovs, K. Krumins, A. Ozols, and D. Pikulins, "Study of the Operational Properties of Bistable Smectic-A Liquid Crystal Displays", *Latvian Journal of Physics and Technical Sciences*, vol. 55, no. 3, pp. 54—62, 2018, doi: 10.2478/lpts-2018-0021. (**Scopus**)
- M. Maltisovs and D. Pikulins, "Study of Electrical Properties of Bistable Smectic-A Liquid Crystal Displays", *Latvian Journal of Physics and Technical Sciences*, vol. 56, no. 5, pp. 3—11, 2019, doi: 10.2478/lpts-2019-0026. (**Scopus**)
- M. Maltisovs, K. Krumins, A. Ozols, and D. Pikulins, "Identifying Defects in Bistable Smectic-A Liquid Crystal Displays After Extended Period of Functional Testing", *2020 IEEE 61st International Scientific Conference on Power and Electrical Engineering of Riga Technical University (RTUCON)*, Riga, Latvia, 2020, pp. 1—5, doi: 10.1109/RTUCON51174.2020.9316559. (**IEEE Xplore**)

- M. Maltisovs, K. Krumins, A. Ozols, and D. Pikulins, "Resolving Defects in Bistable Smectic-A Liquid Crystal Displays", *2020 IEEE 3rd International Conference on Automation, Electronics and Electrical Engineering (AUTEEE)*, Shenyang, China, 2020, pp. 243-247, doi: 10.1109/AUTEEE50969.2020.9315707. (**IEEE Xplore**)

Author has presented the obtained results in the following scientific conferences:

- International Scientific Conference of Environmental and Climate Technologies – **CONECT 2020**, Riga, Latvia, May 13-15, 2020.
- IEEE 61st International Scientific Conference on Power and Electrical Engineering of Riga Technical University – **RTUCON 2020**, Riga, Latvia, November 5—7, 2020.
- IEEE 3rd International Conference on Automation, Electronics and Electrical Engineering – **AUTEEE 2020**, Shenyang, China, November 20—22, 2020.

2. SMART GLASS DEVICES

2.1. Active devices

Smart glass, smart windows or switchable glass have voltage dependent optical properties which can be altered by application of specific electrical signals. These technologies include *EC*, *SPD* and *PDLC* devices. Each of these types has different operating principles, advantages and disadvantages.

Smart glass is dynamic, allowing a traditionally static material to become alive and multifunctional. This technology allows for the control of various forms of light, including visible light, *UV*, and *IR*. Privacy glass products are based on technologies that allow transparent materials (like glass or polycarbonate) to switch, on demand, from clear to shaded or completely opaque (Fig. 2.1). The technology can be integrated into windows, partitions and other transparent surfaces in various sectors, including architecture, interior design, automotive, smart retail windows, and consumer electronics [7].

(a) (b)

Fig. 2.1. (a) — When off, particles are scattered creating opacity for privacy, shading, solar control, or video projection; (b) — when on, particles align, creating transparency for an open atmosphere and natural light [7].

2.1.1 *Smectic-A LC* cells

Most *LC* devices are monostable, with only one possible state in the absence of an electric field. They require a permanent applied voltage and frequent image refreshment, increasing energy consumption. To solve this problem, the use of a bistable display becomes a possibility, where the image (information) is memorized for a long period of time, hence enabling the power consumption to be lowered, similar to electrochromic devices [8].

SmA LC cells offer some important benefits — they can be operated without polarizers, leading to higher light transmittance, improved contrast and remove the need for *LC* alignment control in manufacturing process. The *SmA LC* is switched between a light transparent state (homeotropic orientation) and an opaque light scattering state (focal-conic texture) by applying an external field with various frequencies (see Fig. 2.2).

The stability of the optical states in zero electric field comes from a combined effect of the layered structure of the *SmA* phase and relatively high viscosity of the materials, enabling electro-optic devices, energy efficiency [9].

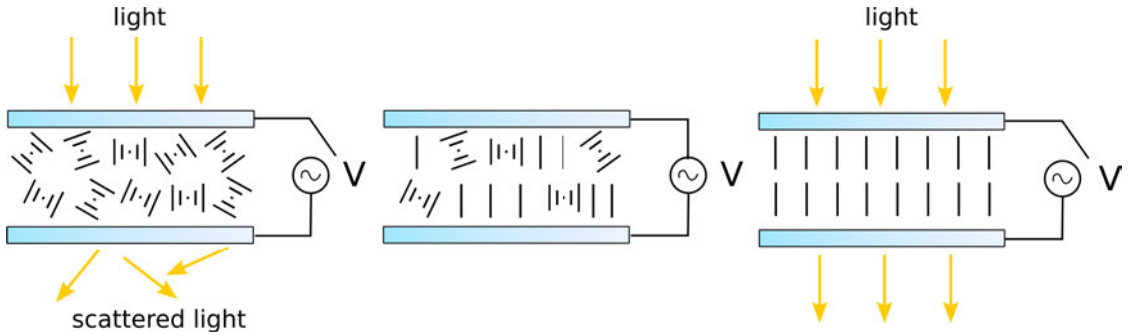

Fig. 2.2. Bistable *SmA LC* cell switching sequence: from the left — light scattering state (electric field is not applied); *LC* switching in progress (electric field is applied); and light transmittance state (*LC* cell is fully switched from one state to the other) [10].

Bistable *Smectic-A LC*) cells have been manufactured by *EuroLCDs Ltd.* (see parameters in Table 2.1). *LCDs* have 300 × 400 mm outer dimensions and active area equally divided into 8 or 25 pixels (see Fig. 2.3). *LC* cell pixels can be switched individually or as a single unit if all the pixels are connected in parallel [11], [12] (see Fig. 2.4 for passive matrix driving technique). To maintain a constant cell gap, 15 µm plastic ball spacers with density of 10 pcs/mm^2 have been used. *LCs* have been supplied by *Dow Corning Corporation* [13], [14].

Table 2.1

SmA LC cell characteristics

Dimensions	300 × 400 mm
Spacer Size	15 µm
Liquid Crystal Type	*Smectic-A*
ITO Resistance	80 Ω/sq

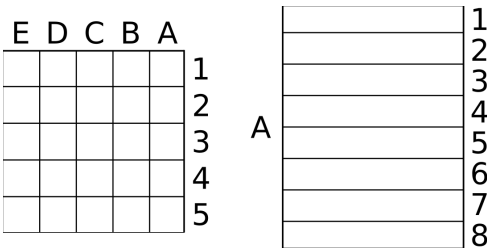

Fig. 2.3. Graphical representation of *LC* cell physical design types. On the left - 5 × 5 pixel and on the right 8 × 1 design.

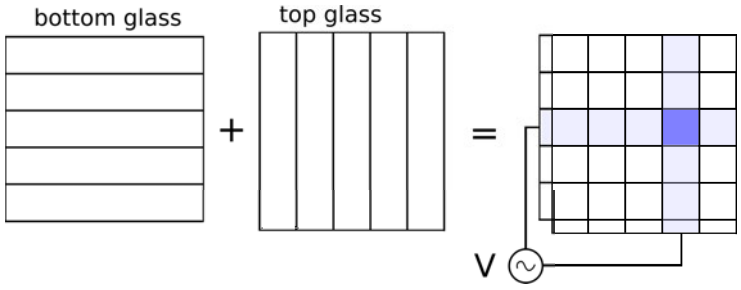

Fig. 2.4. Simplified schematic representation of passive matrix driving technique.

2.2. Operational properties

2.2.1 Frequency response of *LC* cell

Frequency response is one of the key elements that allows product to be characterized and compared to others. It provides important knowledge about *SmA LC* switching threshold levels, as well as the most suitable frequencies to reach the highest light transmittance at transparent state and the lowest light transmittance at scattering state. For the frequency response measurements two different design types of *SmA LC* cells have been manufactured. The main difference was in the dielectric (isolation) coating application procedure: for half of the cells the dielectric coating (Silicon dioxide SiO_2) was applied before *ITO* ablation process, and for other half — dielectric coating was applied after *ITO* ablation (see Fig. 2.5). Contacts were soldered on top and bottom electrodes.

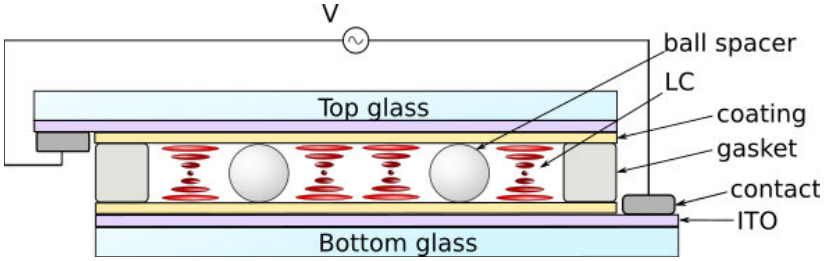

Fig. 2.5. Schematic picture of *LC* cell: cross-section [15].

Three samples from each design type were used in the experiments (see *LC* cell parameters in Chapter 2, section 2.1.1). The reference frequencies — 1 kHz for switching to the transparent state and 50 Hz for switching to the scattering state were chosen on the basis of the *LC* manufacturer's recommendations [13], [14].

The operating voltage 13 V/µm (195V) was determined in manufacturing process during dielectric boundary tests. Experimental setup, shown in Fig. 2.6 and 2.7, consisted of:

1) *SmA LC* cell;
2) optical lenses and white *LED* light source;
3) optical lenses and photodiode (VTB–1013BH with maximized response through the visible part of the spectrum utilized as light detector);
4) high-voltage wires;
5) low voltage and signal wires;
6) *USB* communication cable, PC;
7) optical parameter measurement platform (*OPMP*), allows the measurements of light transmission and switching speed;
8) alternating high voltage source (*AHV*), provides necessary voltage level for creating electric field to switch the *SmA LC* cells.

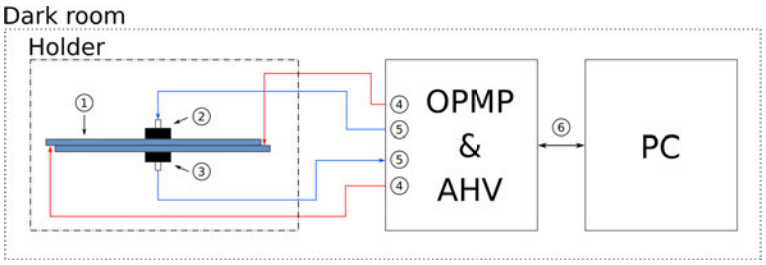

Fig. 2.6. Graphical representation of *SmA LC* cell testing setup.

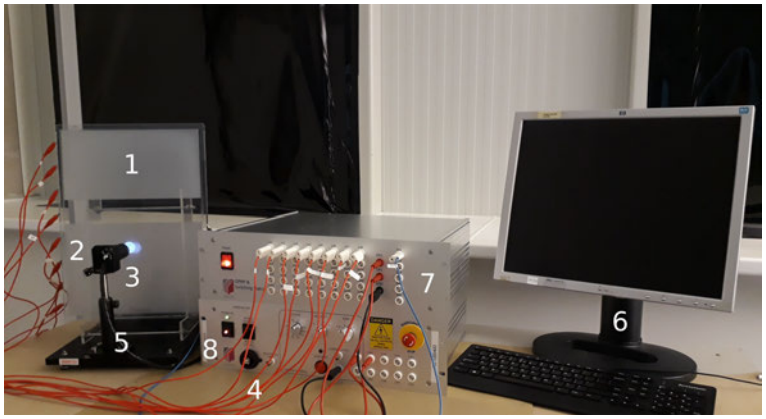

Fig. 2.7. Overview of the experimental setup used for functional testing of *SmA LC* cells.

The obtained *SmA LC* frequency response is shown in Fig. 2.8. The light transmittance depends on switching frequency, i. e., *SmA LC* cell is frequency dependent, which requires specific Hz and signal waveform to reach certain light transmittance values. In Fig. 2.8 the blue curve represents switching from transparent to scattering state and the orange curve — switching from scattering to transparent state.

The frequency range for switching to scattering state is very narrow (10—60 Hz) compared to the frequency range for switching to the transparent state (200—1.5 kHz). *SmA LC* cell could not fully change its state within frequency 5—15 Hz range, and above 50 Hz light transmittance starts to increase rapidly. The inner state can be achieved within 60—100 Hz frequency range, i. e., *SmA LC* cell will stay in-between light scattering and transparent state. The peak of the light transmittance ($>$ 85 %) for switching to transparent state can be reached only in frequency range between 500 Hz and 1.5 kHz, then it will stay within 85.4—86.1 % range.

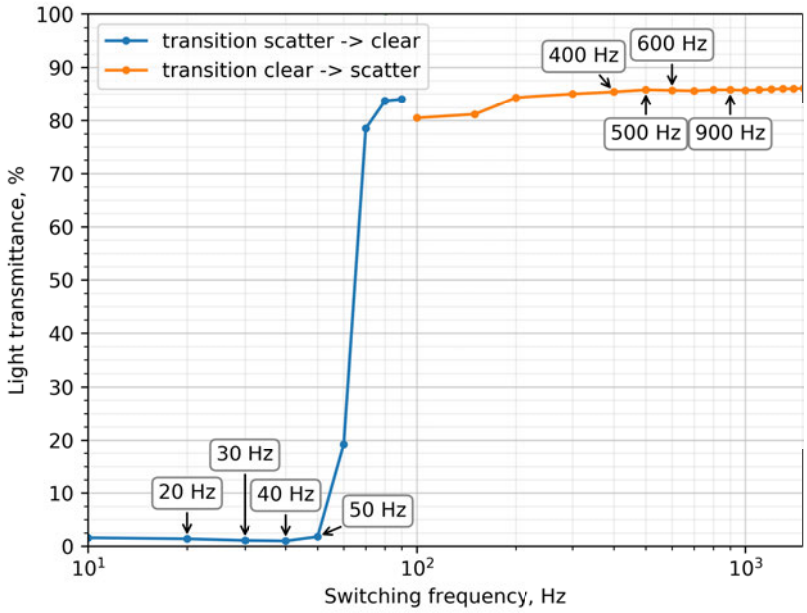

Fig. 2.8. Light transmittance at different switching frequencies.

The more detailed Fig. 2.9 shows a close-up of the frequency response for the light scattering state (blue curve) and another important design parameter — switching speed (orange curve). The main focus in this figure is frequency range 10-50 Hz, since 60-100 Hz will set *SmA LC* cell in the inner state. To achieve the highest switching speed ($\approx$ 1300—1700 ms) and the lowest light transmittance ($\approx$ 1—1.8 %) in scattering state, *SmA LC* should be switched within 20—40 Hz frequency range. The switching speed starts to change rapidly from 20 Hz ($\approx$ 1300 ms) up to 50 Hz ($\approx$ 2200 ms). From 70 Hz and up to 100 Hz switching speed does not change. Maximum driving time was set to 5 s, and in this period *SmA LC* did not show any signs of leaving the inner state, and the light transmittance varied within 20—70 % range. The *SmA LC* cell cannot have both — fast switching speed from state to state and low or high light transmittance — i. e., the driving parameters should be optimized in order to have either responsive switching or good optical properties.

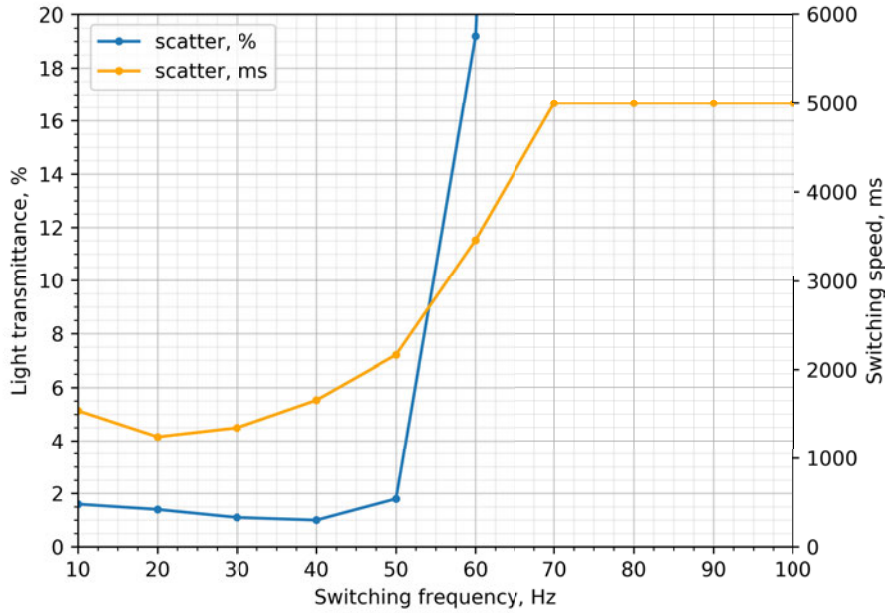

Fig. 2.9. Switching speed (orange) and light transmittance (blue) at different switching frequencies during transition to scattering state.

The second detailed Fig. 2.10 shows a close-up of the frequency response for the transparent state. The light transmittance (blue curve) remains relatively constant ($>$ 85 %) across the 100—1.5 kHz frequency range. From 100 Hz and up to 250 Hz *SmA LC* cell will stay in the inner state, never fully reaching transmittance or scattering state.

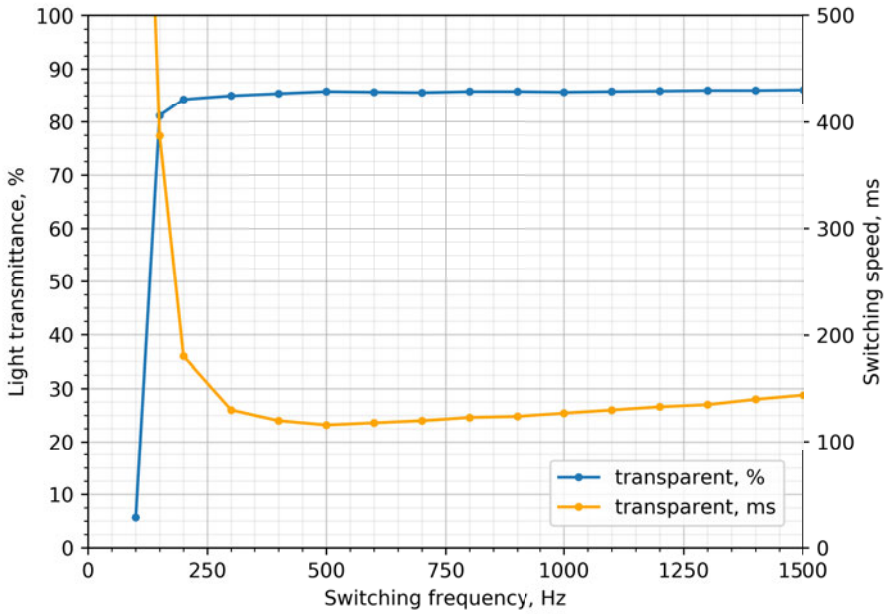

Fig. 2.10. Switching speed (orange) and light transmittance (blue) at different switching frequencies during transition to transparent state.

The switching speed (orange curve) from 100 Hz and up to 500 Hz decreases from ≈ 400 ms to ≈ 115 ms, but from 500 Hz up to 1.5 kHz raises linearly up to ≈ 150 ms. The 400—700 Hz frequency range could be the most suitable for switching *SmA LC* cell to a transparent state, where the light transmittance stays within 85 % and the switching speed varies between 115—150 ms.

2.2.2 Electrical parameters of *LC* cell

Voltage, current and wattage must be clarified in order to electrically characterize the product and compare it to others. The results from the frequency response measurements were analysed and a conclusion was made to update the driving frequencies from scattering state 50 Hz to 30 Hz and transparent state 1 kHz to 600 Hz to obtain better optical parameters and switching response. The updated and the *LC* manufacturer's recommended driving frequencies were used for voltage and current measurements. The voltage was measured at an output of an *AHV* source (see Fig. 2.11) and on the *SmA LC* cell to verify if cables used for connection and/or *LC* cell will create any voltage drops. Current measurements were done with and without external resistors, i. e., external resistors were used to limit the *SmA LC* cell current. For the current limitation 10 different external metal oxide film resistors with resistances ranging from 8.2 Ohm to 330 Ohm (according to the *E24 standard*) were used. This allowed to determine the minimum amount of the required current to fully switch the *SmA LC* cell from transparent state to scattering state and vice versa. Voltage and current measurements were done for eight pixels (whole *LC* cell area), six pixels (6/8 area), four pixels (4/8 area), two pixels (2/8 area) and one pixel (1/8 area).

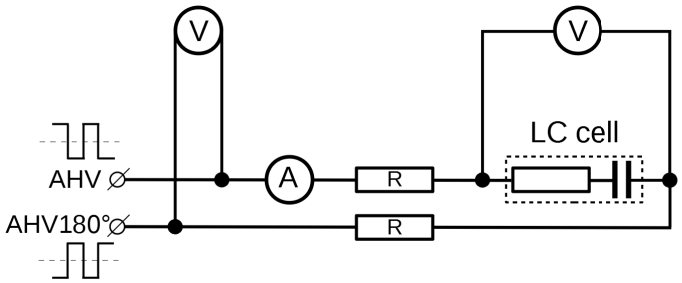

Fig. 2.11. Experimental setup for *SmA LC* cell current limitation and measurements.

The results from voltage and current measurements were analysed, the consumed power (*RMS*) and watt-hours (Wh) were calculated and they are shown Fig. 2.12. The switchable *SmA LC* cell area was adjusted by connecting adjacent pixels in parallel. The power consumption increases exponentially depending on the number of pixels being used. The power consumption reaches the highest point during the transition to a transparent state whilst the whole *SmA LC* cell area is switched. The consumed watt-hour for one switching to the transparent state for a full *LC* cell is ≈ 0.11 Wh, e. g., for 15 switching

times it would be ≈ 1.65 Wh, compared to an average *LED* bulb (8.5 W equivalent to 60 W incandescent bulb) ≈ 0.07 Wh. A *SmA LC* cell consumes approximately the same power amount as two 8.5 W *LED* bulbs.

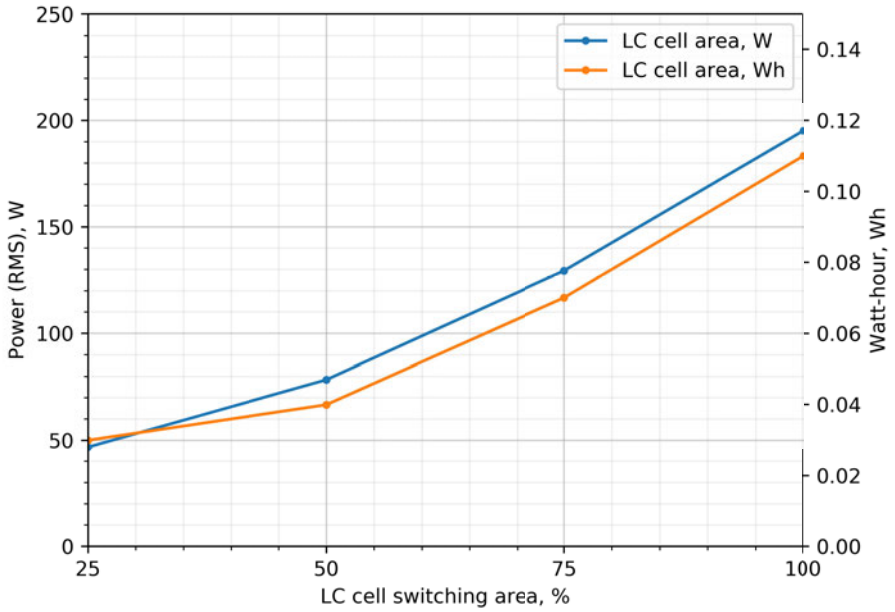

Fig. 2.12. Consumed power (*RMS*) based on the *LC* cell's switching area.

The comparison between 600 Hz and 1 kHz is shown in Table 2.2, for 30 Hz and 50 Hz in Table 2.3.

Table 2.2

Comparison of Consumed Power between 600 Hz and 1 kHz

Driving Frequency	**Voltage**	**Peak Current**	***RMS* Current**	**Peak Power**	***RMS* Power**	**Transmittance**
600 Hz	190 V	3.12 A	1.03 A	588.21 W	194.42 W	85.10 %
1 kHz	190 V	3.14 A	1.33 A	590.74 W	249.94 W	85.02 %
	Difference:	**0.64 %**	**22.56 %**	**0.43 %**	**22.21 %**	

Table 2.3

Comparison of Consumed Power between 30 Hz and 50 Hz

Driving Frequency	**Voltage**	**Peak Current**	***RMS* Current**	**Peak Power**	***RMS* Power**	**Transmittance**
30 Hz	190 V	3.10 A	0.26 A	581.13 W	49.29 W	1.52 %
50 Hz	190 V	3.09 A	0.29 A	579.92 W	55.05 W	1.74 %
	Difference:	**0.32 %**	**10.34 %**	**0.21 %**	**10.46 %**	

The current measurements with additional current limiting resistors are shown in Fig. 2.13. The measurements were done for 8 pixels (whole LC cell area), four pixels (4/8 area), two pixels (2/8 area) and one pixel (1/8 area). The SmA LC cell (8 pixels) require at least 0.9 A of current to switch the whole area from scattering to transparent state and obtain $>$ 85 % light transmittance.

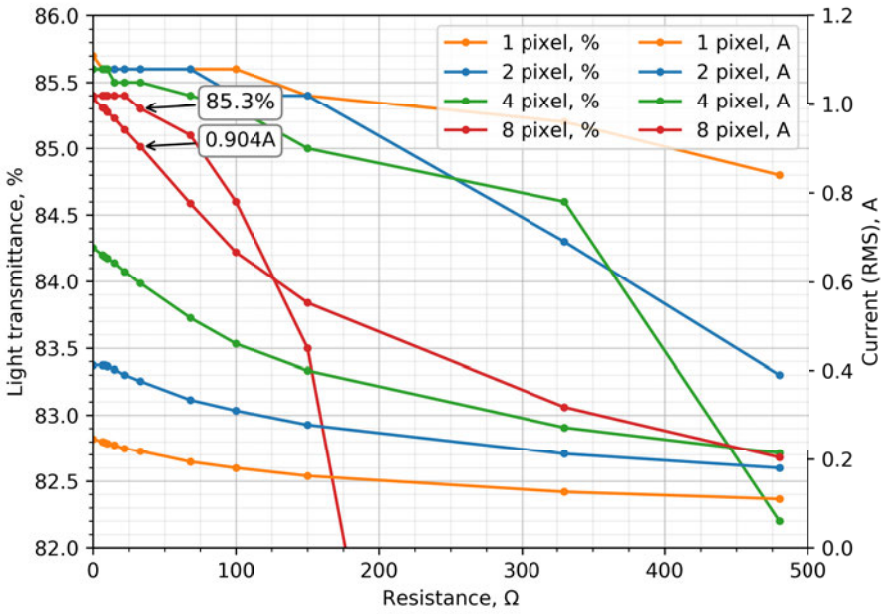

Fig. 2.13. Current measurements with current limiting resistors.

To achieve lower peak current, the LC cell can be switched sequentially (pixel by pixel or pixel groups), but the switching speed must be taken into account. For example, in order to switch 8 pixels to the scattering state it takes up to 5 s and $\approx$ 0.9 A, but if the LC cell is switched 4 times by 2 pixels, it will take up to 3—5 s and $\approx$ 0.3 A per group switching.

2.3. Long-term switching problems

2.3.1 Functional testing

Every product that has been developed needs to be tested to verify and validate the design and development processes. It is necessary to make sure the product is safe for customer, complies with necessary product, product group and manufacturing standards, and performs the function it is required to perform.

LCDs and LC cells go through various stages of testing, e. g., functional, parameter variation testing, Product Development Testing (PDT), Highly Accelerated Life Testing ($HALT$), Qualification Tests (QT), Failure Oriented Accelerated Testing ($FOAT$), Burn In Test (BIT) [16], [17], [18]. All of the testing methodologies have been thoroughly

analysed and improved by some manufacturers and research laboratories. These testing stages are adaptive, i. e., same testing principles could be used for other products as well, to obtain the best results each of the stages should be modified to the specific product needs. However, there are no better or worse, each testing methodology play crucial role in products quality, performance, maintenance, etc.

After the assembly process *SmA LC* cells go through the first electrical testing, where *LC* breakdown boundaries are clarified. It is necessary to determine the *LC* cell maximum operating voltage, so that a system that operates with this type of *LC* cell in normal operational and fault conditions would never reach this critical boundary.

When the *LC* cell breakdown thresholds are acknowledged, operational properties must be determined (both — clear, scatter frequencies and operating voltage) [19] in order to obtain the highest light transmittance in a transparent state and the lowest in a scatter state. Switching speeds and power consumption must not be forgotten, because end the device should be energy efficient and responsive.

All the *SmA LC* cells were tested with the same parameters (see Table 2.4) and one full functional testing cycle consists of:

1) switching to the scatter state and the operational parameter measurement;
2) pause between state-state switching;
3) switching to the transparent state and the operational parameter measurement;
4) pause between state-state switching;
5) pause between switching cycles.

Table 2.4

SmA LC Cell Functional Testing Parameters

Measurement frequency	500 Hz
Measurement time	4 s
Measurement angle	0 °
Switching voltage	13 V/µ (195 V)
Switching waveform	DC balanced square wave
Scatter state frequency	30 Hz
Transparent state frequency	600 Hz
Switching time (scatter)	3 s
Switching time (transparent)	1.5 s
Pause between state-state	2 s
Pause between cycles	5 min

Each one was switched at least 1000x (full cycles), that took around 40 hours to complete. Altogether 20 *LC* cells were tested over more than 30 day period of time. Every 100+ cycles the measurements were stopped and the *LC* cells were photographed to see if any visual changes occurred.

LCDs and *LC* cells are functionally tested in different environments, one of which is the dark room. In such a room it is possible to minimize the error in the optical transmittance measurements due to the constant lightning. But it is not always possible to provide a constant room temperature unless a climate chamber is used where it can be set to constant value. Climate chambers are used to make sure that the developed product will be able to function completely at different extreme humidity and temperature levels. These tests are carried out to obtain maximum functionality limits so that the user knows in what type of environment the product can be used without damaging it. In this case, the temperature was dependent on the settings of the building's ventilation system. In Table 2.5 environmental parameters are listed.

Table 2.5

The Environment in which the Experiments were Conducted

Premises	dark room
Lighting	constant
Temperature	room temperature

The experimental setup used for extended functional testing was the same as the one mentioned in the Chapter 2.2, section 2.2.1.

2.3.2 Obtained defects

The figures below show the most common defects that appeared during and were detected after the extended period of functional testing. In Fig. 2.14 *SmA LC* cell with 5 × 5 design were tested. To be more precise, only one pixel (*C3*) was switched 1000+ times from state to state and pixels around it were observed to understand the impact on them. Before the testing was started, initial pixel states were set, i. e., pixel *C2* and *C3* was switched to the transparent and pixel *C4* to the scatter state.

After the functional testing pixel *C2* remained still in transparent state. Near the pixels' perimeter, parts of the active area have changed to scatter state, i. e., near laser ablation lines (pixel separation lines) the area unevenly changed from transparent to scatter state. Additionally, random *LC* clusters (from distance visually looked like dots) are randomly switched to scatter state, *C2* pixel looks dotted.

Pixel *C3* transmittance has decreased by ≈ 0.4 % and not completely changed its state to transparent at the end of extended period of functional testing. *C3* perimeter,

just like *C2*, has unevenly changed from transparent to scatter state. The centre of the pixel *C3* looks visually smooth and even, and there are no noticeable *LC* clusters.

In Fig. 2.14 pixel *C4* is partially visible, but its initial state has not changed, i. e., still in light scattering state. By looking closely at the figure, it is possible to see that near laser ablation lines pixel has unevenly started to change to transparent state. Similarly to *C2*, pixels' *C4* area near ablation line *LC* clusters have randomly switched to transparent state.

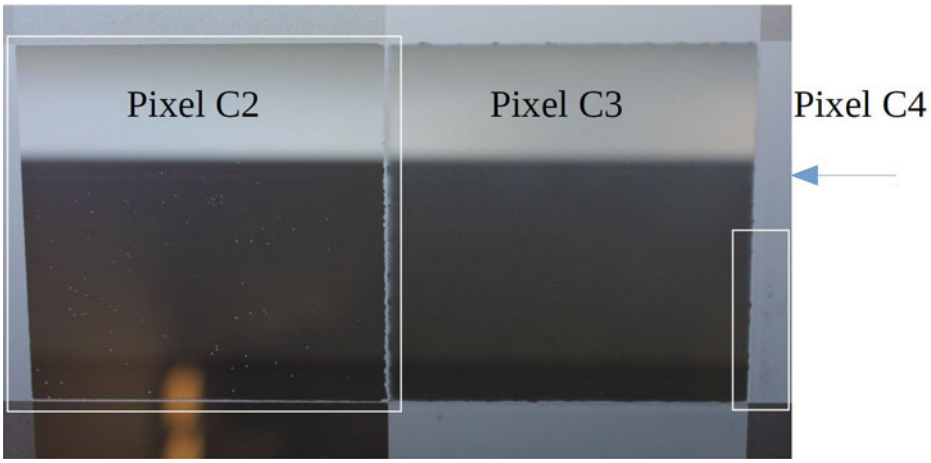

Fig. 2.14. *SmA LC* cell (5 × 5 design) close-up of the three middle pixels — *C2*, *C3* and *C4*.

Fig. 2.15 (a) and (b) are the close-up of Fig. 2.14 captured with the microscope. In Fig. 2.15 it can be seen that the *LC* cluster zones around the *C3* perimeter are not completely switched to transparent state. Pixels *C2* and *C4* were not grounded during the functionality testing of pixel *C3*. From obtained results, it can be concluded that the electrical field impacts the pixel that is next to the pixel that is being switched from state to state. Also *LC* tends to get stuck near the pixels, perimeter (cannot change its state completely), and with time (if pixel switching routine does not change) the small *LC* clusters tend to get bigger and start to form larger un-switched areas.

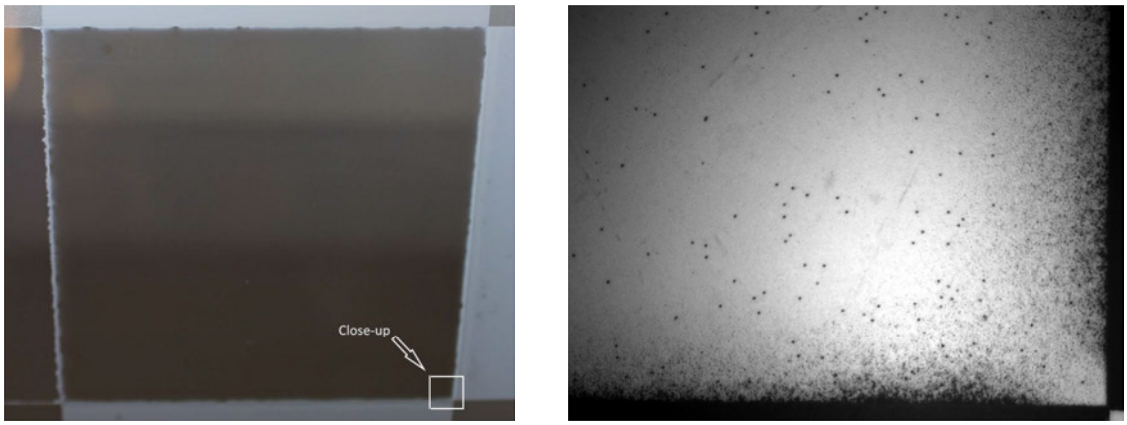

(a) (b)

Fig. 2.15. *SmA LC* cell (5 × 5 design): (a) — close-up of the middle pixel *C3*; (b) — lose-up of the lower right corner of pixels C3 captured with microscope.

The second common defect that appeared was brighter laser ablation lines, compared to the rest of the *LC* cell area or pixel it self. This defect was especially evident in the *SmA LC* cell 8 × 1 design. In Fig. 2.16.(a) it can be seen that pixel laser ablation lines are brighter than the rest of the pixels' area, and the pixels' outline looks wavy, the edges are visually rugged. The rest of pixels' area is uniform, there are no random *LC* clusters, etc.

In Fig. 2.16.(b) laser ablation lines are more pronounced, i. e., they are more scattered (with lower light transmittance) than the rest of the *SmA LC* cells' area. The *LC* cell has not completely changed its state to scatter, all of the active area is wavy and not uniform. Near laser ablation lines both types of the *LC* clusters can be observed, i. e., bigger and smaller *LC* clusters that are changed to transparent and scatter states.

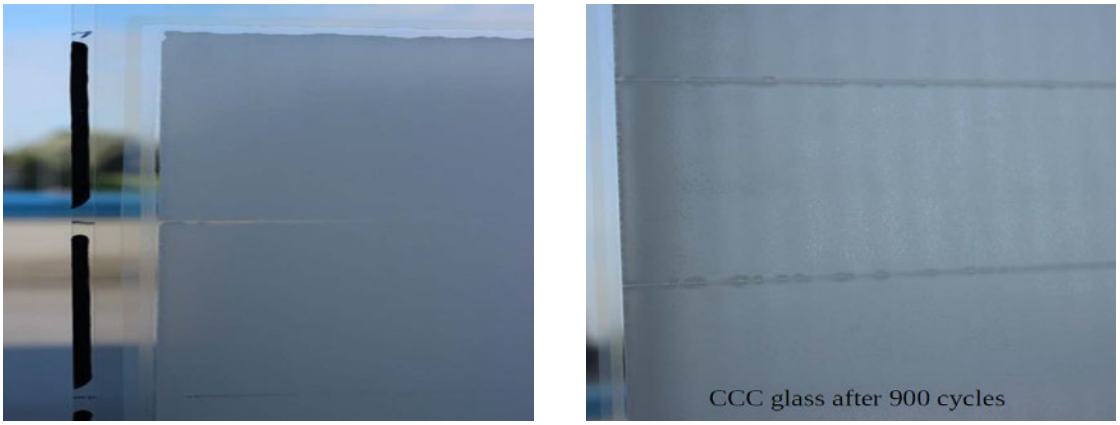

(a) (b)

Fig. 2.16. *SmA LC* cell (8 × 1 design): (a) — close-up of pixels laser ablation lines and outline; (b) — close-up of pixels, active areas and laser ablation lines.

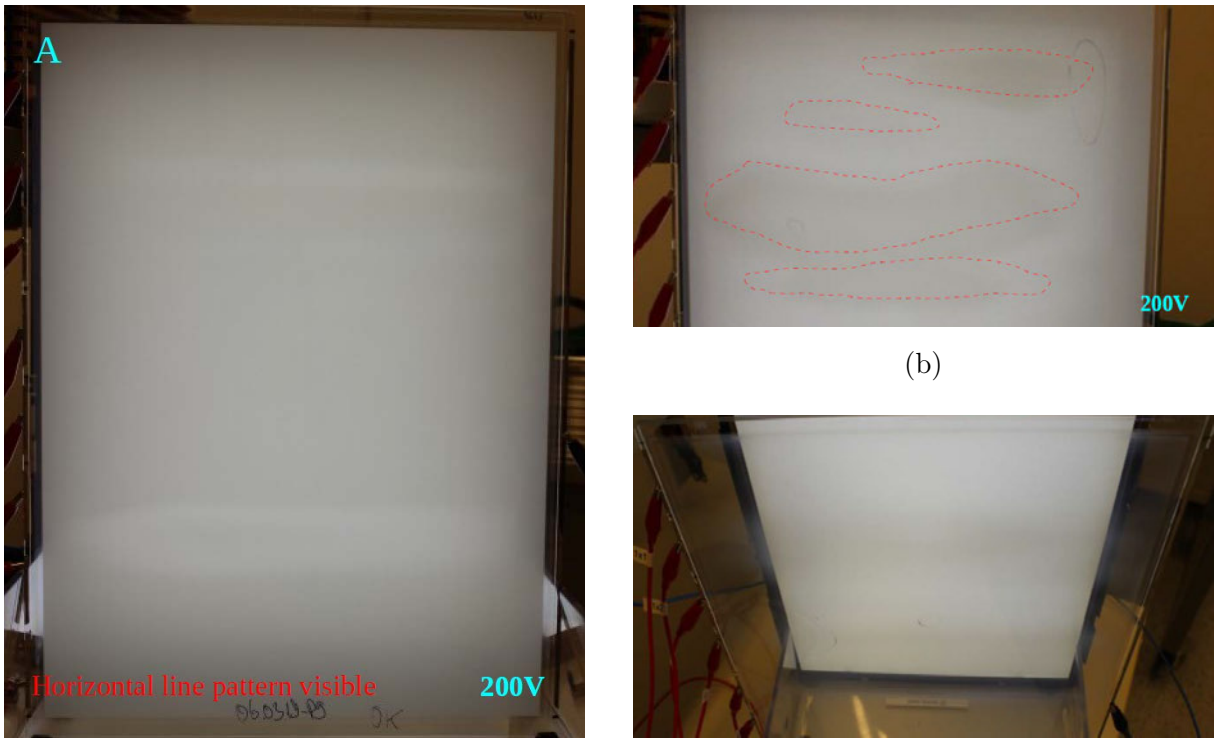

(a) (b) (c)

Fig. 2.17. *SmA LC* cell (8 × 1 design): (a) — close-up of the scatter state; (b), (c) — close-up of the transparent state. Additional background (behind the *LC* cell) lightning was used for better visual defect identification.

2.4. Defect resolving

2.4.1 Testing cycle and parameter optimization

Without extended research it is impossible to optimize the switching parameters for *SmA LC* cells, therefore three different experimental series were performed. The first experiment was devoted to understand if testing cycle and parameter optimization could resolve different defects that were described in Chapter 2.3, Section 2.3.1 and prevent their appearance in long term. All *SmA LC* cells were tested with the same parameters (Chapter 2.3, Section 2.3.1).

Figure 2.18 shows one of the most common defects, i. e., random *LC* cluster zones in the middle of the pixels' active area. When *LC* molecules are in the lowest energy state and weak electric field is applied, *LC* molecules due to the low rotational force start to create random *LC* clusters. Uneven thickness of the *SmA LC* cell, inappropriate switching parameters or testing cycle could be the reasons why the defect occurred.

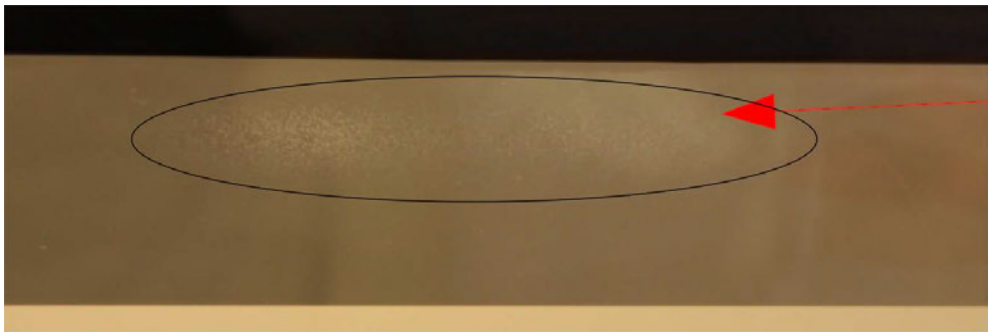

Fig. 2.18. Unswitchable (stuck) LC cluster zones in inner state before testing cycle and parameter optimization.

In this case, to eliminate and fix this defect, it is necessary to optimize the driving voltages and update the testing cycle sequence. Additional pauses should be added between pixel-pixel and state-state switching. Also different switching voltages should be used for each switching state. The obtained results are shown in Fig. 2.19 and parameter comparison — in Table 2.6.

Updated functional testing cycle consists of:

1) Switching to the scatter state and the operational parameter measurement.
2) Pause between pixel-pixel switching.
3) Pause between state-state switching.
4) Switching to the transparent state and the operational parameter measurement.
5) Pause between pixel-pixel switching.
6) Pause between state-state switching.
7) Pause between switching cycles.

Table 2.6

SmA LC Cell Optimized and Non-optimized Switching Parameter Comparison

	Before	**After**
Measurement frequency	500 Hz	
Measurement time	4 s	
Measurement angle	0 °	
Switching voltage (scatter)	13 V/µ (195 V)	
Switching voltage (transparent)	13 V/µ (195 V)	9 V/µ (135 V)
Switching waveform	DC balanced square wave	
Scatter state frequency	30 Hz	
Transparent state frequency	600 Hz	
Switching time (scatter)	3 s	7.5 s
Switching time (transparent)	1.5 s	
Pause between pixel-pixel	0 s	1 s
Pause between state-state	2 s	5 s
Pause between cycles	5 min	

Recommendations would be to start with the switching time and then with pause extension optimization. If switching time and pause extension does not work, additional pauses in-between pixel-pixel switching and state-state must be added. Switching voltage optimization must be used as the last option, because it will require to change the switching timings and pauses once again, see Fig. 2.20.

Fig. 2.19. Unswitchable (stuck) *LC* cluster zones disappeared after testing cycle and parameter optimization.

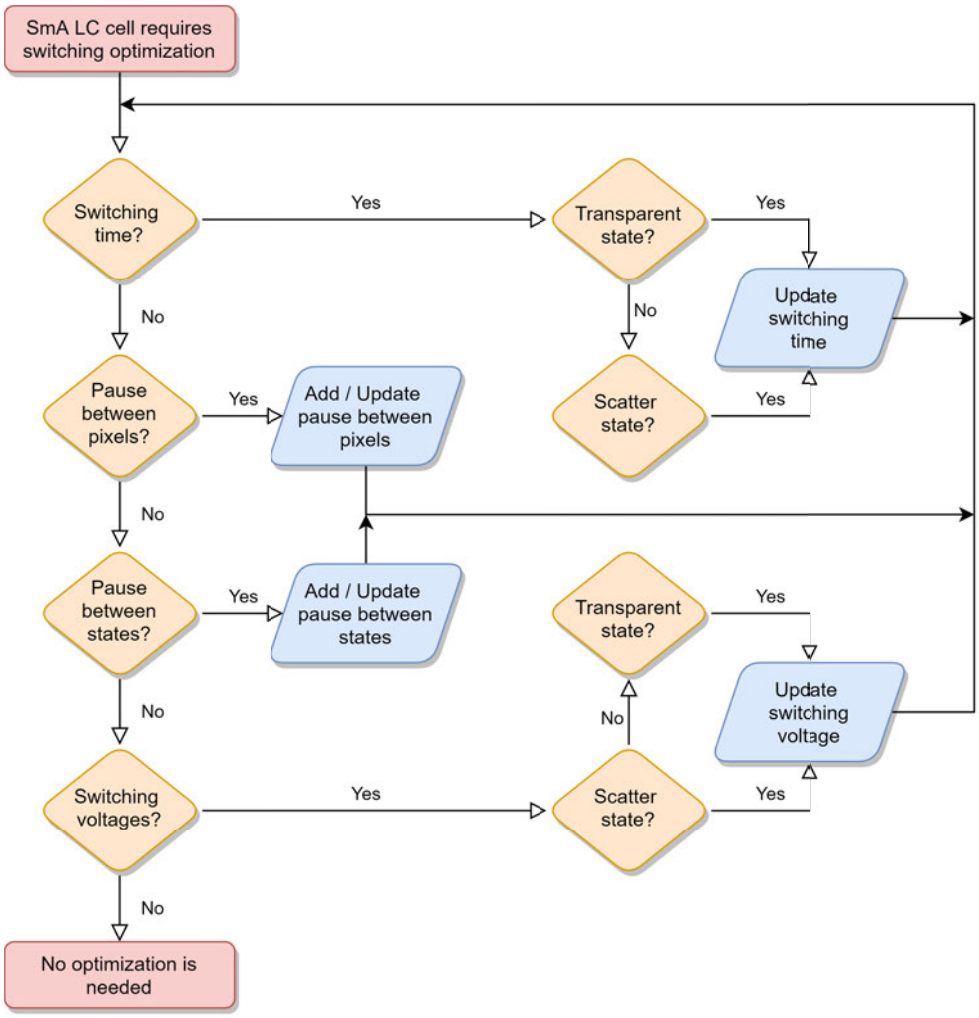

Fig. 2.20. *SmA LC* cell switching optimization diagram.

With switching parameter and testing cycle optimization it is possible to improve visual conditions of different defect, e. g., pixels, wavy outline and rugged edges. These defects tend to return after X number of cycles, but are less pronounced (see Fig. 2.21). The needs of end user experience and visual look of a finished product must be taken into account, e. g., if *SmA LC* cell is mounted into 2—to—3 chamber PVC window, then the available active area will reduced by ∼2—5 % with black isolation material and pixels, wavy outline and rugged edges will not be visible.

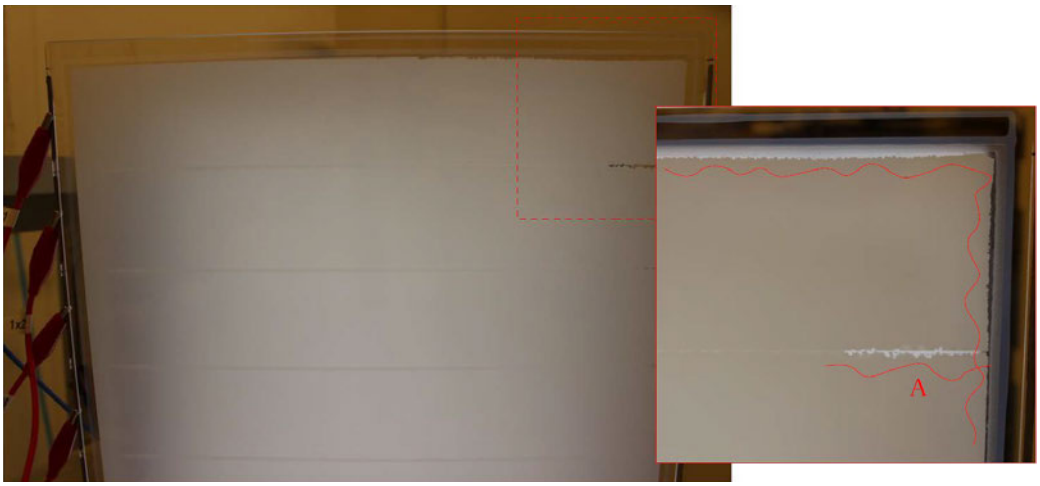

Fig. 2.21. Defected *SmA LC* cell — pixels with wavy outline, rugged edges and unfixable separation line between two pixels.

Near laser ablation lines (pixel separation lines) unevenly changed area from transparent to scatter state can only be partially improved, none of the experiments, testing methods and optimizations showed any potentials to completely eliminate this problem. With the naked eye it is practically impossible to see this defect in transparent sate, but in scatter state with special attention to the lines, the defect can be noticed.

Similar result was obtained for uneven (discoloured) active area and was partially improved. The defect is related to the production of the display and the methods used there. Manufacturing processes must be optimized to avoid such a defect (see Fig. 2.22).

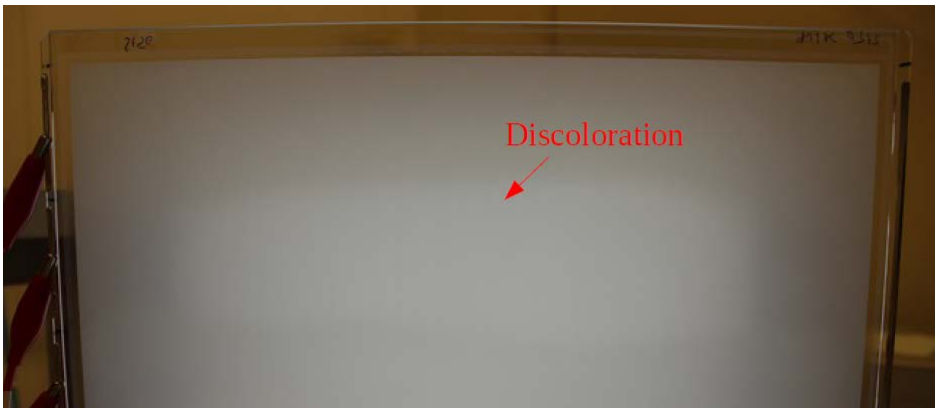

Fig. 2.22. Discoloured pixels, active area of *SmA LC* cell in light scattering state. Additional background (behind the *LC* cell) lightning was used for better visual defect identification.

2.4.2 Switching waveform optimization

In order to realize such an experiment, additional equipment was needed, because the *AHV* (alternating high voltage source) used in previous experiment could generate only a DC balanced square wave signal with different amplitudes and timing periods. High voltage power supplies, signal generator, operational amplifier and other equipment can be seen in Fig. 2.23, but simplified functional schematic in Fig. 2.24.

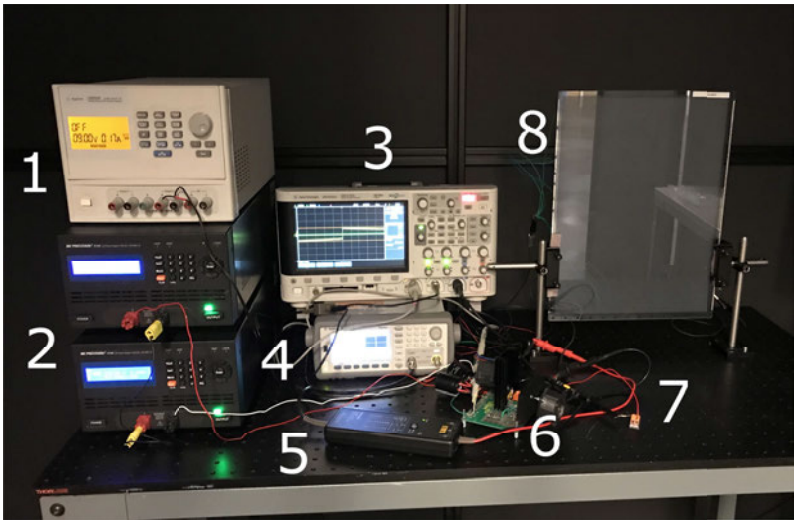

Fig. 2.23. Overview of the experimental setup used for switching waveform optimization for *SmA LC* cells. Used equipment: 1 – Agilent U8032A; 2 – B&K Precision 9184; 3 – Agilent DSOX2014A; 4 – Agilent 33500B; 5 – Tektronix P5200; 6 – Apex PA93; 7 - textitRx (current measurement resistor), 8 – *SmA LC* cell.

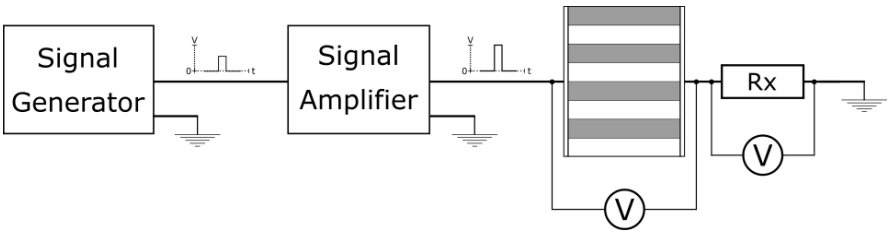

Fig. 2.24. Simplified functional schematic of electrical parameter measurement setup, where waveform generator generates sine wave, sawtooth or other custom signal, signal amplifier amplifies switching signal from 100 V up to ±2 00 V and outputs it to textitSmA LC cell and additional Rx resistance.

Different switching waveform experiments were held to understand if with other type of waveforms better optical parameters or higher switching speeds would be achievable. To properly switch the *SmA LC* cell from state-state, the switching signal must be DC balanced, therefore, sine and triangle signal waveform generation, as well as amplification was tested.

Multiple units were tested with three different switching signals, but the switching voltages, pauses between pixel-pixel and state-state, switching timings, etc. remained unchanged. The obtained results are quite interesting, see Tables 2.7 and 2.8, because units could change their states with DC balanced square and sine wave signals, but with triangle *SmA LC* cell stuck in the inner state and stayed there.

Sine wave results are similar to square wave, but with improvements in electrical parameters, i. e., less current and power is required to switch the *SmA LC* cell, meaning — lower energy consumption and lower maintenance costs in long term use case. The downside are worse optical parameters, in transparent state light transmittance decreased by $\approx$ 4—8 %, but in scatter state it increased by $\approx$ 6—10 %.

Table 2.7

Switching Waveform Experiment — Transparent State

Signal	**textitRMS, A**	**Peak, W**	**textitRMS, W**	**Energy, Wh**	**Close**
Square	0.11—0.12	198—207	22—23	0.25—0.26	1.3—1.4
Sine	0.14—0.16	135—157	29—32	0.09—0.15	7.5—11.2
Triangle	N/A	N/A	N/A	N/A	N/A

Table 2.8

Switching Waveform Experiment — Scatter State

Signal	**textitRMS, A**	**Peak, W**	**textitRMS, W**	**Energy, Wh**	**Close**
Square	0.23—0.25	287—306	46—48	0.18—0.26	85.3—85.6
Sine	0.07—0.08	135—157	13—15	0.05—0.06	10.5—14.4
Triangle	N/A	N/A	N/A	N/A	N/A

2.4.3 Other defect resolving methods

The third experiment was carried out to understand if temperature treatment in pre-heated industrial oven would "reset" or remove the defects that appeared during extended functional testing or with inappropriate switching cycle and/or testing parameters, see Fig. 2.25.

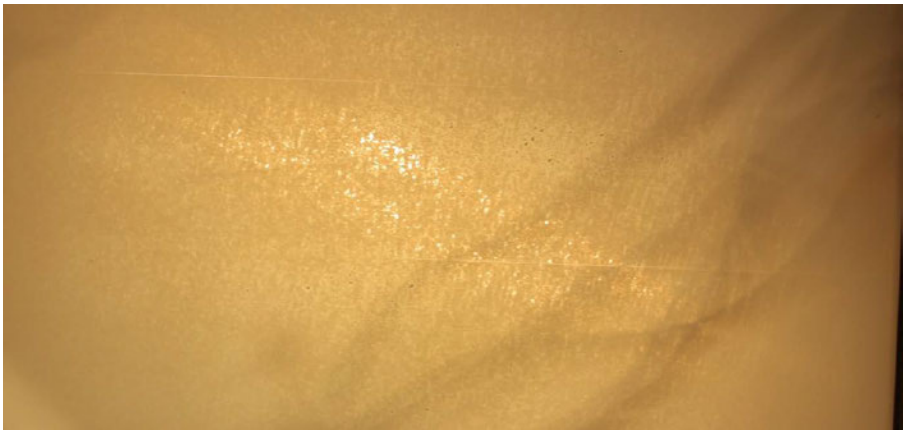

Fig. 2.25. Unswitchable (stuck) *LC* cluster before temperature treatment. Darker, brighter and transparent spots resemble inhomogeneities of polyimide coating.

Different switching parameter and testing cycle sequence optimization was done, but without any useful results. In this case the *SmA LC* cell was put into a preheated oven at 100 °C. LC was melted within first 25 minutes, then left in room temperature to cool down; since melted *SmA LC* looks exactly the same as the cooled down, it is hard to tell how long it took to cool down (≈2-3 h) (see Fig. 2.26).

After the *SmA LC* cell was fully cooled down to room temperature. scattering state was visually checked. the *LC* cell looked homogenous again without any defects visible to naked eye. To verify if the *SmA LC* cell is working properly and defects does not appear again, the unit was tested for 100+ cycles with the same switching parameters and testing cycle sequence.

Since this unit was placed in an insulated window package and filled with argon, the only defect that had occurred after heating treatment was the curvature of the outer glass sheets. The visual appearance of the active area was smooth, ablation lines very fine, practically invisible. It functionally switched from state-state and from pixel-pixel without any problems.

(a) (b)

Fig. 2.26. *SmA LC* cell after temperature treatment: (a) — *LC* cell looks clear due to the *LCs*, high viscosity (viscosity changes based on *LCs* temperature), (b) — *LC* cell after 100+ testing cycles, no visual and functional defects were found.

2.5. Electrical simulation model

2.5.1 *ITO* layer and dielectric resistance

The need of a good simulation model for an *LC* cell or *LCD* becomes apparent during the design of driving system. *LC* capacitance is critical in the simulation of *LC* cell or *LCD* pixels and is voltage dependent due to the *LC* characteristics.

Simple parallel *RC* circuits usually represent the behaviour of *LC* cell or *LCD* in a variety of situations. These electric circuits are of great practical interest, since they can be used in countless applications ranging from theoretical studies to simulations of *LC* cell or *LCD* elements [20].

Due to the anisotropy of *LC* material, the *LC* capacitance (C_{LC}) is not constant. It varies from a minimum capacitance when no voltage is applied across the *LC* cell to a maximum capacitance when the *LC* cell is fully turned on [21]. Thus, the *LC* capacitance (C_{LC}) is bias and time dependent. This mechanism has been thoroughly analysed by some *LC* manufacturers and laboratories. However, the formulation is very dependent on the specific *LC* type [21], [22].

The *LC* cell can be considered as an ideal capacitor. Due to its construction, it is very similar to a flat capacitor, where both plates are made up of two *ITO* layers and between them there is *LC* material with ε_r [23]. It is more precise to take into account

conductivity loss and LC cell approximation in a narrow band with a non-ideal capacitor model (Fig. 2.27), where R is the electrical resistance of the output (ITO layer and dielectric) and C is the electrical capacity of a flat capacitor.

By adding additional R and C elements, a model describing the LC cell up to a frequency range of 10^{-1}—10^{7} Hz can be obtained [20].

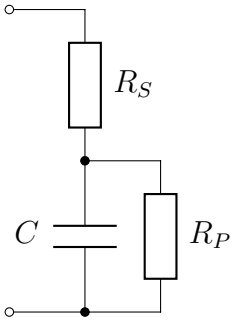

Fig. 2.27. LC cell equivalent electrical circuit.

Equivalent series resistance R_S (Equation ()2.1.)) can be determined by rapidly applying voltage and measuring the voltage on a series-connected resistor ($R_x = 5$—$10\ \Omega$) (Fig. 2.29). At the first moment of time, C is a short circuit and voltage divider is formed. R_S can be calculated as follows:

$$R_S = \frac{(V_s - V_x)R_x}{V_x} \tag{2.1.}$$

The obtained results from the measurements of equivalent series resistance R_S is shown in Figure 2.28. Two different R_x values were used (5.2 Ω, 10.4 Ω). The measurements were made at a number of V_s values ranging from 5 V to 195 V with a 5 V increment step. Blue dots represent $R_x = 5.2\ \Omega$ and orange dots represent $R_x = 10.4\ \Omega$. The green line represents the mean value of both R_x value measurement data.

Pronounced deviation is noticeable in 5 V to 30 V range. When the LC cell is energized, switching is gradually taking place. This is due to the low rotational force caused by the electric field applied to liquid crystal molecules if they are in the lowest energy state. From 40 V to 195 V, R_S does not depend on the applied voltage and $R_S \approx 71\ \Omega$.

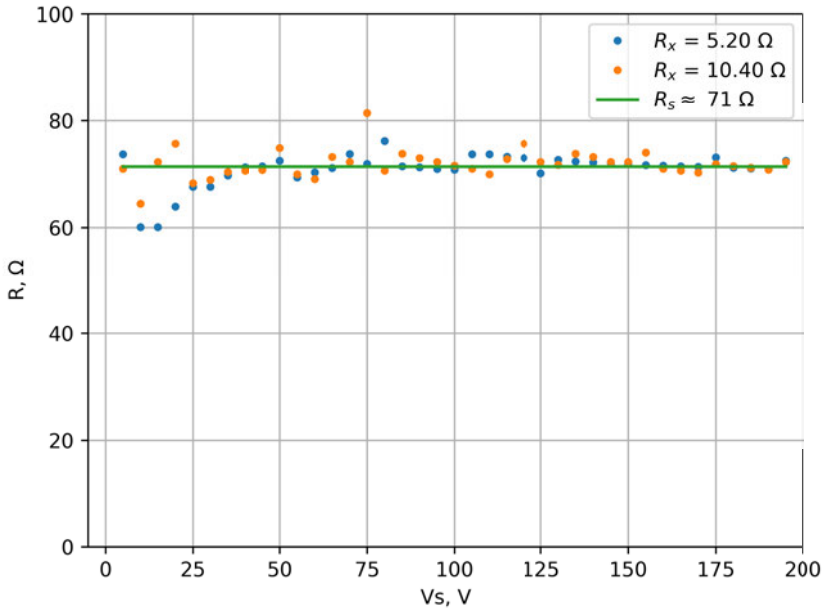

Fig. 2.28. Equivalent series resistance R_S dependence of V_S.

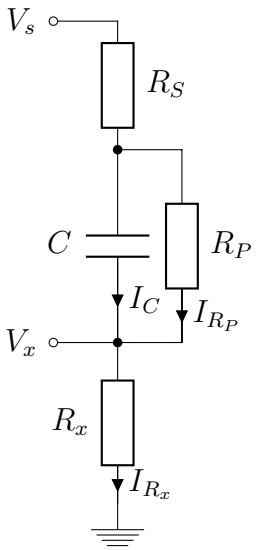

Fig. 2.29. Simplified electrical parameter measurement circuit.

2.5.2 *LC* capacitance

An effect related to reorientation experienced by the LC molecules is change of capacitance offered by a single LC pixel, C_{LC}. Due to the dielectric anisotropy of LC mixture, this capacitance is voltage dependent [23].

In the second experiment, equivalent parallel resistance R_P and capacitance C were determined. In this case V_s was not a rapid voltage step but more gradual and $R_x = 1\text{k}\ \Omega$ (Equation (2.2.)) [15]:

$$\frac{V_x(t)}{R_x} = I_{R_x}(t) = I_C(t) + I_{R_P}(t). \tag{2.2.}$$

After certain amount of time, C is fully charged, $I_C = 0$ *and* $I_{R_x} = I_{R_P}$. Since $R_S \ll R_x$, R_P, then R_P can be calculated according to the voltage divider formula (Equation (2.1.)). When R_P is found I_C can be calculated as follows:

$$I_C(t) = I_{R_x}(t) = I_{R_x}(t) - I_{R_P}(t) = \frac{V_x(t)}{R_x} - \frac{V_s - V_x(t)}{R_P}. \tag{2.3.}$$

Total charge accumulated on the capacitor can be obtained by integrating I_C(t):

$$Q_C = \int I_C(t)dt. \tag{2.4.}$$

Fully charged equivalent capacitor capacity can be calculated as follows:

$$C = \frac{Q_C}{V_s - V_x}. \tag{2.5.}$$

Measured *SmA* LC cell C capacitance change over V_S is shown in Fig. 2.30. Dotted blue line represents C and orange line the mean value of C in LC cells' functional range 100—195 V. Obtained capacitance from 5—40 V $\approx$ 44 nF with a slight drop at 35 V. Then, increasing the V_s, the capacitance increases up to 100 V and $\approx$ 53 nF. With the voltage being continuously increased capacitance change within 10 % range. LC material dielectric permeability depends on the position of molecules and can be influenced by the external electric field. The capacitance dependence of the applied electric field is not linear.

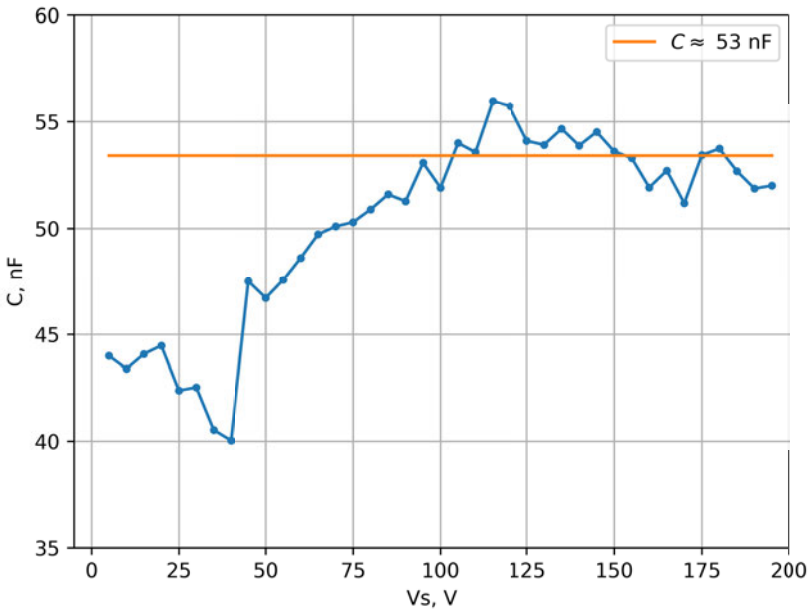

Fig. 2.30. LC cell capacitance C dependence on V_S.

2.5.3 *LC* resistance

An *LC* with high viscosity needs high intensity electric field for operation, but in this case an *LC* electrical breakdown is likely to occur. Electrical breakdown in the cell is observed when the electric field intensity E in the *LC* layer is above a specific breakdown value E_{br}. The E_{br} is governed by the conductivity of the *LC*, surface smoothness of the electrodes, defects in coatings as well as point defects, such as dust particles, in the *LC* layer. The dielectric breakdown in an *LC* cell is a complicated process discussed elsewhere [24]. Based on the parameters of the equivalent electrical circuit, it is possible to calculate power dissipation on R_S and R_P:

$$P_{R_S}(t) = I_x^2(t) * R_S = R_S * \frac{V_x^2(t)}{R_x^2}. \tag{2.6.}$$

$$P_{R_P}(t) = \frac{U_c^2(t)}{Rp} = \frac{(V_s(t) - V_x(t) * (1 + \frac{R_S}{R_x}))^2}{R_P}. \tag{2.7.}$$

The obtained results of equivalent parallel resistance R_P are shown in Fig 2.31. Dotted blue line represents measured R_P and orange line is the calculated mean value of R_P in *SmA* *LC* cell functional range 100—195 V. From 5 V and up to 20 V there is an increase in resistance as it should be with different *LC* materials (example *Cholesteric LC*) were R_P increase up to 1 MΩ. In this case rapid decrease follows and parallel resistance decreases to ≈ 13.5 kΩ and from 125—195 V stays within 5 % deviation. The low resistance is explained by the difference of the *LC* composition itself.

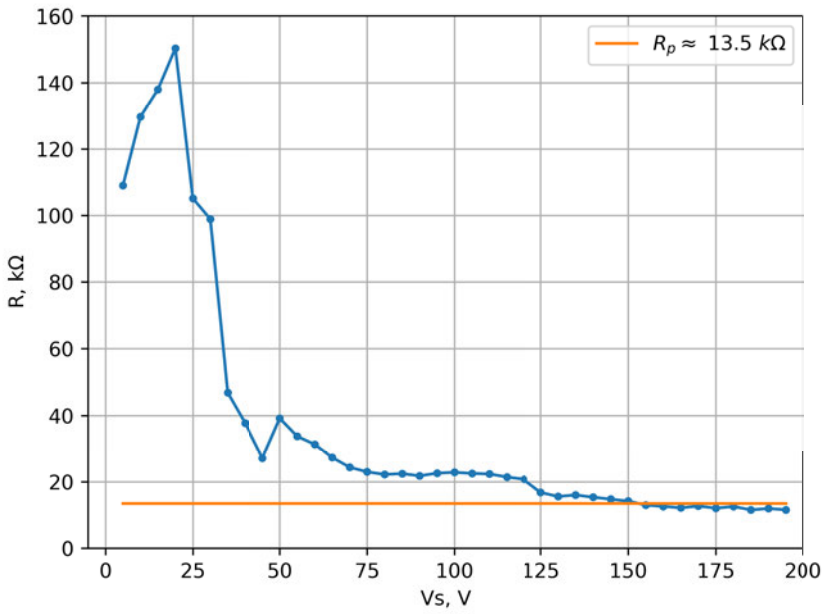

Fig. 2.31. Equivalent parallel resistance R_P dependence on V_S.

Obtained power dissipation results on R_S and R_P are shown in Fig. 2.32. Dotted orange line represents R_P and blue — R_S resistance. At 195 V, V_S, which is the typical operational voltage of *SmA* LC cells, $R_S \approx 2.1$ W and $R_P \approx 6.3$ W. Both the equivalent parallel and series resistance shows exponential growth. Most of the power is dissipated on R_P. R_P can be reduced by minimizing V_S voltage; however, this would affect the LC cell switching speeds and optical parameters. R_S cannot be reduced due to the proportional current required by the LC cell to charge its equivalent capacity.

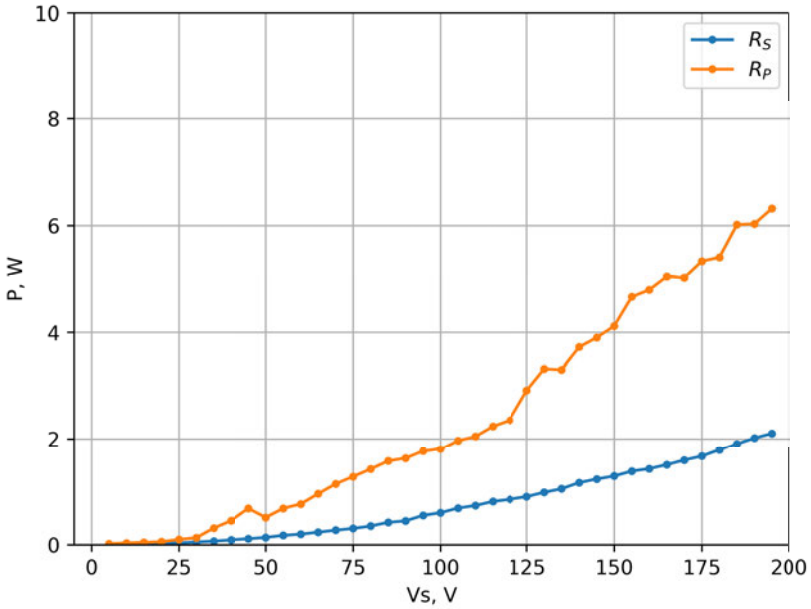

Fig. 2.32. R_S and R_P power dissipation dependence on V_S.

CONCLUSIONS

The aim of the Doctoral Thesis was to provide research on the *SmA LC's* functional behaviour and potential to become the next generation product, that could improve society's daily life. The author has obtained the following results:

1. **The light transmittance and switching speed on *SmA LC* cells, depending on the switching frequency was explored.** *SmA LC* cell is frequency dependent, which requires specific Hz and signal waveform to reach certain light transmittance values. The frequency range for switching to scattering state is very narrow (10—60 Hz) compared to the frequency range for switching to the transparent state (200—1.5 kHz). The inner state can be achieved within 60—100 Hz frequency range, i. e., *SmA LC* cell will stay in-between the light scattering and transparent state. **To achieve the highest switching speed ($\approx$ 1300—1700 ms) and the lowest light transmittance ($\approx$ 1—1.8 %) in scattering state *SmA LC* should be switched within 20—40 Hz frequency range. And the 400—700 Hz frequency range is the most suitable for transparent state, where the light transmittance stays within 85 % and the switching speed varies between 115—150 ms.**
2. **Power consumption was explored based on the switching area.** The power consumption increases exponentially depending on the number of pixels being used. The power consumption reaches the highest point during the transition to a transparent state whilst the whole *SmA LC* cell area is switched. **The consumed watt-hour for one switching to the transparent state for a full *LC* cell is $\approx$ 0.11 Wh, e. g., a *SmA LC* cell consumes approximately the same power amount as two 8.5 W *LED* bulbs. The *SmA LC* cell (8 pixels, 300 $\times$ 400mm) require at least 0.9 A of current to switch the whole area from scattering to transparent state and obtain $>$ 85 % light transmittance.**
3. **Switching differences between different *LC* cell design types was explored.** *SmA LC* cells with 8x1 designs tend to have more pronounced laser ablation lines, i. e., *LC*, near these lines, with time will have better optical properties — lower light transmittance compared to the rest of pixels' active area. Pixels, edges tend to be more rugged than straight line. 5 $\times$ 5 design or similar chess patterned layouts will have problems with switching sequence, image or text displaying. *LC* tends to create zones and clusters near laser ablation lines. Pixels that are next to the pixel that is being switched, will start to randomly change their state and create random LC clusters. SmA LC cells are sensitive to the switching parameters, due to the low parallel resistance, they tend to warm up with intensive switching from state to state. Switching speed rises and *LC* cell stays within the inner state. *SmA LC* cells will never often and quickly change their states without

specified pause in-between switching steps — only in cases where testing procedure requires to understand the LC degradation boundaries.

4. ***LC* defect types, their appearance reasons and possible solutions was explored.** In addition to previously mentioned 8×1 and 5×5 design defects, *SmA* LC cells had non uniform active area, some with wavy pattern. Visually sharp light scattering differences, LC did not completely change its state, stuck in the inner state (LC clusters with different light transmittance values near each other). In both states (transparent and scatter) these regions could not be completely switched to either state. **With switching parameter and testing cycle optimization it is possible to improve visual conditions of different types of defects, by adding additional pauses (1—5 s) between pixel-pixel and state-state switching, e. g., pixels, wavy outline and rugged edges.** These defects tend to return after X number of cycles, but are less pronounced. Unevenly changed area from transparent to scatter state near the laser ablation lines can only be partially improved, none of the experiments, testing methods and optimizations showed any potentials to completely eliminate this problem. With the naked eye it is practically impossible to see this defect in transparent sate, but in scatter state with special attention to the lines, defect can be noticed. Similar result was obtained for uneven (discoloured) active area and was partially improved. The defect is related to the production of the display and the methods used there. Manufacturing processes must be optimized to avoid such a defect. Temperature treatment proved that it is possible to "restart" the *SmA* LC cell after being damaged with incorrect switching parameters, testing sequence or other unknown source. This method should be used only if the defect could not be fixed with switching optimization. The procedure should be tested and verified with defected LC cells to understand if other type of defects could also be fixed.
5. **Equivalent load representation options for electronic sub-system simulations was explored.** Obtained results of series R_S and parallel resistance R_P show that $\mathbf{R_S}$ **stays within provided *ITO* tolerances (± 20 %)** and does not depend on the applied voltage. R_P resistance is lower compared to other LC cell parallel resistance, e. g., cholesteric LC cell. Great attention should be paid to the power dissipation, because with such a low internal parallel resistance LC can quickly reach its temperature limit and *SmA* LC cell will stop working. **Capacitance C measurements provide information about SmA LC cells' functional range 100-195 V, at which the applied electric field is high enough to be able to rotate *LC* molecules and change *LC* state from transparent to scattering and vice versa.** Additional in-depth research should be done in 5—95 V range to fully understand the LC molecule threshold voltage at which they start to rotate. **Simulation model parameters $R_S = 71\ \Omega$, $R_P = 13\ \text{k}\Omega$, $C = 53$ nF will provide sufficient information**

about electric functionality of the large size 300 × 400 mm *SmA LC* cell and can be integrated into the development of larger systems. This methodology can also be adapted to other *LC) cell types and used to create new electric simulation models.*

BIBLIOGRAPHY

[1] S. Lu and D. H. Davies, "THERMALLY AND ELECTRICALLY ADDRESSED DYE SWITCHING LCDs." *Molecular crystals and liquid crystals*, vol. 94, no. 1-2, pp. 167–189, 1983.

[2] A. Hochbaum, "Thermally Addressed Smectic Liquid Crystal Displays," *Optical Engineering*, vol. 23, no. 3, jun 1984.

[3] K. Liu and K. H. Yang, "ELECTRODE CONFIGURATIONS TO REDUCE THE POWER CONSUMPTION AND ENHANCE THE CONTRAST OF THE MATRIX-ADDRESSED SMECTIC A LIQUID CRYSTAL DISPLAY." *IBM technical disclosure bulletin*, vol. 27, no. 7 B, pp. 4145–4148, dec 1984.

[4] D. F. Aliev, V. L. Aristov, V. V. Mitrokhin, and V. P. Sevostyanov, "Operating characterization of a smectic A LCD," *Displays*, vol. 12, no. 2, pp. 86–90, 1991.

[5] S. S. Seomun, Y. Takanishi, K. Ishikawa, H. Takezoe, and A. Fukuda, "Evolution of switching characteristics from tristable to V-shaped in an apparently antiferroelectric liquid crystal," *Japanese Journal of Applied Physics, Part 1: Regular Papers and Short Notes and Review Papers*, vol. 36, no. 6 A, pp. 3586–3590, 1997.

[6] V. L. Aristov, S. P. Kurchatkin, M. V. Mitrokhin, and V. P. Sevostyanov, "Electrohydrodynamic formation of liquid crystal focal conic domains," in *Liquid Crystals: Physics, Technology, and Applications*, vol. 3318. SPIE, feb 1998, p. 529.

[7] Gauzy, "Smart Glass - Everything You Want To Know...And More." [Online]. Available: https://www.gauzy.com/smart-glass-everything-you-want-to-know/

[8] J. Bin Lias, T. Naing Oo, T. Yazawa, M. Kimura, and T. Akahane, "Liquid crystal alignment on patterned-alignment films," *Journal of Information Display*, vol. 12, no. 2, pp. 101–107, 2011. [Online]. Available: https://doi.org/10.1080/15980316.2011.567826

[9] J. W. Huh, T. H. Choi, J. H. Kim, J. H. Woo, J. H. Seo, and T. H. Yoon, "Bistable Switching of Diffractive Smectic-A Liquid Crystal Device between Haze-Free Transparent and High-Haze Translucent States," *ACS Photonics*, vol. 5, no. 8, pp. 3152–3158, aug 2018.

[10] G. Mozoļevskis, "DIELECTRIC BREAKDOWN OF HIGH VOLTAGE LIQUID CRYSTAL DISPLAYS," Ph.D. dissertation, RIGA TECHNICAL UNIVERSITY, Riga, 2017.

[11] D. J. Cristaldi, S. Pennisi, and F. Pulvirenti, *Liquid Crystal Display Drivers: Techniques and Circuits*, 1st ed. Springer Science+Business Media B.V., 2009. [Online]. Available: http://www.springer.com/gp/book/9789048122547

[12] E. Lueder, *Liquid Crystal Displays: Addressing Schemes and Electro-Optical Effects*, 2nd ed. Wiley, A John Wiley and Sons, Ltd, Publication, 2010. [Online]. Available: https://www.wiley.com/en-lv/Liquid+Crystal+Displays{\%}3A+Addressing+Schemes+and+Electro+Optical+Effects{\%}2C+2nd+Edition-p-9780470688182

[13] T. V. Clapp, W. A. Crossland, A. B. Davey, M. Grassman, J. P. Hannington, R. K. King, M. Pivnonenko, S. Robson, and H. Xu, "Liquid crystal formulations and structures for smectic a optical devices," p. 85, 2011. [Online]. Available: http://www.dowcorning.com/content/paintink/paintinkresin/default.aspx

[14] J. P. Hannington, T. V. Clapp, F. Nishida, R. K. King, O. Farooq, M. Grassman, W. A. Crossland, H. J. Coles, A. B. Davey, H. Xu, O. Hadeler, and M. Pivnenko, "Oligosiloxane modified liquid crystal formulations and devices using same (US Patent)," p. 28, 2013.

[15] G. Mozolevskis, A. Ozols, E. Nitiss, E. Linina, A. Tokmakov, and M. Rutkis, "Reduction of Electric Breakdown Voltage in LC Switching Shutters," *Latvian Journal of Physics and Technical Sciences*, vol. 52, no. 5, pp. 47–57, 2015.

[16] K. R. Fowler, *Test and Integration.* Elsevier Inc., 2015. [Online]. Available: http://dx.doi.org/10.1016/B978-0-12-405879-8.00014-3

[17] H. Grzeskowiak, T. Lhommeau, and D. Delaux, "Highly Accelerated Testing," *Reliability of High-Power Mechatronic Systems 2: Aerospace and Automotive Applications Issues, Testing and Analysis*, pp. 57–108, 2017.

[18] E. Suhir, J. Nicolics, and S. Yi, "Failure-oriented-accelerated-testing and its role in making a device into a product," *2019 IEEE International Workshop on Metrology for AeroSpace, MetroAeroSpace 2019 - Proceedings*, pp. 33–38, 2019.

[19] M. Maltisovs, K. Krumins, A. Ozols, and D. Pikulins, "Study of the Operational Properties of Bistable Smectic-A Liquid Crystal Displays," *Latvian Journal of Physics and Technical Sciences*, vol. 55, no. 3, pp. 54–62, 2018.

[20] H. Aoki, "Dynamic characterization of a-Si TFT-LCD pixels," *IEEE Transactions on Electron Devices*, vol. 43, no. 1, pp. 31–39, 1996.

[21] B. Bahadur, *Liquid Crystals — Applications and Uses, Vol. 1.* Singapore: World Scientific Pub Co Inc., 1990. [Online]. Available: https://www.worldscientific.com/worldscibooks/10.1142/1013

[22] T.-H. Choi, S.-M. Do, B.-G. Jeon, and T.-H. Yoon, "Low-power control of haze using a liquid-crystal phase-grating device with two-dimensional polymer walls," *Optics Express*, vol. 27, no. 3, p. 3014, 2019.

[23] G. Karmakar, S. Roy, G. Chattopadhyay, and Z. Xiao, "Dynamically controlling exterior and interior window coverings through IoT for environmental friendly smart homes," *Proceedings - 2017 IEEE International Conference on Mechatronics, ICM 2017*, pp. 487–491, 2017.

[24] C. Neusel and G. A. Schneider, "Size-dependence of the dielectric breakdown strength from nano- to millimeter scale," *Journal of the Mechanics and Physics of Solids*, 2014.

Matīss Maltisovs was born in 1991 in Madona. He obtained a Bachelor's degree (2013) and professional Master's degree (2015) in Electronics from Ventspils University of Applied Sciences. From 2014 to 2017 he was a product/process engineer at EuroLCDs, from 2017 to 2018 he was a guest lecturer. From 2018 to 2021 he was an electronics engineer at HansaMatrix Innovation. Currently he is an electronics engineer at Lightspace Technologies. His research interests include smart glass/ windows and power electronics.